

Measuring Entropy in Mesoscopic Circuits

by

Owen Sheekey

A THESIS SUBMITTED IN PARTIAL FULFILLMENT
OF THE REQUIREMENTS FOR THE DEGREE OF

Honours Bachelors of Science

in

THE FACULTY OF SCIENCE
(Physics)

The University of British Columbia
(Vancouver)

April 2021

© Owen Sheekey, 2021

Abstract

We have tested whether the entropy of a quantum system can be measured nonlocally, using a capacitively coupled quantum dot as a sensor. We have extended upon the research already done in mesoscopic circuits showing that the entropy of the first few electron ground states in a quantum dot can be locally measured directly. To demonstrate whether this local measurement can be extended to measure the entropy of a nonlocal quantum system, we have probe a simple two state system made up of an electron in a superposition between a quantum dot and a reservoir. Entropy measurements were completed by capacitively coupling this two-state system to a probe quantum dot whose occupation affects the degeneracy of the two-state system and by extension, its entropy. In the dot acting as the probe dot, change in entropy of the entire system was measured by measuring shifts in the occupancy transition from 0 to 1 electrons as a function of temperature. By showing that we can measure the entropy of a quantum system nonlocally — or by measuring only the properties of a nearby, coupled quantum dot — we provide a path to distinguish more novel entangled states with unique entropies.

Table of Contents

Abstract	ii
Table of Contents	iii
List of Tables	v
List of Figures	vi
Glossary	xi
Acknowledgments	xii
1 Introduction	1
2 Entropy in mesoscopic systems	3
2.1 Entropy of quantum systems	3
2.2 From a Maxwell relation to entropy	5
2.3 Approximate form for a quantum dot coupled to a thermally broadened lead	6
3 Capacitively coupled double quantum dot	7
3.1 The device and measurement protocol	7
3.2 Entropy of a double quantum dot system	11
3.3 Conclusion	14
A Measurement technique	17

A.1	Heating	17
A.2	Extraction of dN/dT signal	20
A.3	Artifacts from cross couplings	20
A.4	Back action noise	20
A.5	Determination of electron temperature	20
B	Measurement setup	23
C	Device Fabrication	26
C.1	Summary	26
C.2	Recipes	27
C.2.1	Gallium removal	27
C.2.2	Mesa Etch	27
C.2.3	Ohmic contact	28
C.2.4	Gating	29
C.2.5	Disclaimer	30
Bibliography		32

List of Tables

Table 3.1 Entropy along 01, 10 transition	12
Table C.1 Evaporation for ohmics	28

List of Figures

- Figure 2.1 In (a) a simple potential well is shown, with the energy levels of various occupations plotted on top of the potential diagram. In (b) and (c) a transition from $0 \rightarrow 1$ electrons in the potential well is illustrated. In (c) finite temperature broadening of this transition, as well as a shift in μ_{system} , due to the change in entropy of the transition, is shown as temperature increases (still much too small to allow for excited states).

Figure 3.1 A cross sectional view of the AlGaAs/GaAs substrate used in measurements for this thesis. A stack of GaAs and AlGaAs forms a 2 dimensional electron gas (2DEG) at their interface. Ohmic contact is made to the 2DEG by a thermal annealing process with Ni/Au/Ge further discussed in C.2. Gold (Au) top gates are defined on the surface of the substrate which allow for local control of the density of the 2DEG.

Figure 3.2 A top-down SEM image of the device measured in this experiment. Lighter gold regions are the gold gates, while darker regions are the GaAs substrate. A single quantum dot (right hand side) is probed by the leftmost dot whose occupation is measured using I_{sense} . In this device, temperature oscillations occur across electrons in a reservoir connected to the probe dot heated via a small thermocurrent through an adjacent quantum point contact. V_{ACC} is used to control the chemical potential, μ , in the probe dot. In the right dot, similar gate structures, labelled V_{IP} allow for the system to be tuned to be tuned degenerate with the probe dot. The X indicates ohmic contact to the 2DEG. The light red section indicates the thermal reservoir of the system. Greyed out gates were not used in this experiment.

9

Figure 3.3 In (a) and (b) we show two examples of the measurement protocol where the occupancy of the probe dot is measured using I_{sense} . In each case, the occupancy is swept from $N - 1$ to N electrons both at a higher temperature (red) and a lower temperature (blue), however in (a) this change in N does not correspond to an entropy change in the system whereas in (b) we see a positive change in entropy of the system due to this change in occupancy. The inlaid plots show the cumulative integral of dI_{sense} – or the difference between hot and cold I_{sense} curves. The entropy change of the system is measured by the value of this integral after the completion of this transition. Figure adapted from [7].

11

Figure 3.4 In (a) the states of the double quantum dot system are mapped out by charge sensing the occupation of both dots. The color indicates the derivative of the current through the charge sensor. Sudden changes in this current indicate state changes in the two dots, with larger changes (seen as darker on this plot) indicating changes in the main dot, and smaller changes (slightly lighter on this plot) indicating changes in states in the impurity dot. The large squares indicate regions of constant state in the two dots and are labelled by [occupation main dot, occupation impurity dot]. In (b), a zoomed in view on the crossing (white circle in plot (a)) of the $0 \rightarrow 1$ transitions in the two dots is shown.

12

Figure 3.5 Entropy along the $0,1 \rightarrow 1,0$ transition in the pair of dots with $\Gamma_{main}/T < 1 < \Gamma_{imp}/T$. In (a) the dark region indicates the transition in the main quantum dot. Double dot states are labelled as [Occupation main dot, occupation impurity dot]. The ΔS of the transition in the main dot is plotted for the double dot transition crossing. In the $0,0 \rightarrow 1,0$ regime, the ΔS is found to be roughly $\ln 2 \approx 0.69$ as expected from the spin degeneracy in the probe dot. In the central regime, where there is a full $0,1 \rightarrow 1,0$ transition, entropy is found to be around $\ln 2 - \ln 2 = 0$ since the spin degeneracy of the impurity dot is simply replaced by the spin degeneracy in the probe dot. In (b) the ΔI between the cold and hot curves plotted in (c) are shown. In (c) the shift in V_{mid} between 70 mK and 50 mK traces can clearly be seen to vary depending on ΔS .

15

Figure 3.6 Entropy along the $0,1 \rightarrow 1,0$ transition in the pair of dots with $\Gamma_{main}/T \approx \Gamma_{imp}/T < 1$. In (a), dI_{sense}/dV_{ACC} indicates the state of both dots as a function of V_{IP} . In (b), theoretical calculations of ΔS are plotted along with the experimental values, error bars showing 95% confidence interval. In (c) dN/dT in units of dI_{sense}/dT is plotted.

16

Figure A.1 In (a) the double dot system from measurements in this thesis is shown on a top-down false-color scanning electron microscope (SEM) image. In (b) the relation of this device to the other components of the heating apparatus are shown on another top-down SEM image. The two stage heating is labelled by T_{hor} : stage 1, then T_{mid} : stage 2. A number of quantum point contact (QPC)s control the connection between these stages including the HQPCs which are used for heating, the SQPC which is the source of heat for the second stage, and the DQPC which is the drain for the second stage.

19

20

Figure A.2

Figure A.3 By fitting the transition line shapes of the $0 \rightarrow 1$ electron transition in the quantum dot, one can extract the broadening of the fermi energy in the reservoir. By varying the lattice temperature of the substrate and plotting the effective broadening of the fermi sea (θ) at each lattice temperature, we can extract the effective electron temperature, T_e . Here $T_{e,base} \approx 35$ mK. .

22

Figure B.1 In (a) a current power spectral density (PSD) and its integral for an open line are plotted indicating an open line noise of about $200 \text{ fA}/\sqrt{\text{Hz}}$ in the $0 \rightarrow 1$ kHz bandwidth. Notably, the majority of the remaining noise can be attributed to a contribution at 400 Hz which we attribute to a vibrational resonance in our wiring. In (b), the coldfinger design utilized for this low noise setup is imaged. Flat flexible cables are used to connect the wiring to a set of RC filters on the face of the MC plate (top of picture). These cables are spray-coated in a thin layer of graphite which limits vibrations from inducing triboelectric noise in the cables.

24

Figure C.1 In (a), a sample chip is shown (optical image) before (L) and after (R) annealing. Notably, the process of annealing melts the metals that were evaporated onto the surface of the chip, forming an alloy. The change in surface quality of the metal between the two images shows that this process has occurred. In (b) and (c) a sample pair of optical images show a sample with resist having already been written (b) and this same chip post evaporation (c). In (d), a schematic side view of the lithography process is shown. PMMA forms concave side walls preventing the metallic film from making contact with the substrate, except in areas defined by an electron beam. After a state like that shown in (d) is reached, Acetone can be used to “lift off” the unneeded metallic film by dissolving the PMMA on which the metallic film is resting.

31

Glossary

2DEG 2 dimensional electron gas

QPC quantum point contact

SEM scanning electron microscope

PSD power spectral density

MC mixing chamber

Acknowledgments

I would first like to thank all the students in Josh Folk's lab for all they have done for this project and for all they have taught me about being an experimentalist. Christian Olsen, who was patient while I was first learning how to do anything useful in the lab. Manab Kuiry, who discussed physics with me everyday, and is always up to date on all the newest results. And of course, Tim Child, without whom this project would not have been possible.

More here.

Chapter 1

Introduction

In the past few decades, significant advances in the field of quantum transport have yielded a large number of interesting quantum systems and effects including Majorana bound states [12], the 2-channel Kondo effect [17], and the $v = 5/2$ fractional quantum hall state [25]. All of these systems have been well characterized using traditional transport techniques. However, if we were able to measure the entropy of mesoscopic quantum systems like these, we would be able to more clearly distinguish them from trivial states, and perhaps detect deviations from theory in ways which traditional transport measurements do not allow. Of particular interest is the Majorana bound state whose characteristics make it especially well suited to the field of quantum computing [1, 14], but whose transport signature is suspiciously close to that of the much less interesting (and less useful) Andreev bound state [22]. It has been proposed that the entropy of such a Majorana bound state would significantly differ from that of an Andreev bound state [21]. However, in the past, entropy measurements of systems like these were never possible because of limitations of techniques which rely on heat capacity and other macroscopic quantities which can be experimentally difficult to measure for localized quantum states.

A few years ago, Hartman et al. [7] showed that it is possible to measure the entropy of a single spin $\frac{1}{2}$ particle in a quantum dot, opening the possibility of introducing entropy as a new technique for characterization of more interesting mesoscopic quantum systems, like those mentioned above. To complete their measurement, Hartman et al. measured electronic occupation in a few-electron quantum

dot at varying temperatures, relating this quantity to entropy following a Maxwell relation. Recently, schemes similar to the one realized in this experiment have been used to measure entropy in magic angle (twisted bilayer) graphene [18, 19]. Both measurements have shown remarkable evidence of an effective “freezing” of electrons as temperature is increased – analogous to the Pomeranchuk effect in ^3He [16]. The results of these recent experiments further illustrate the value in measurements of entropy in quantum materials to provide insights into the electronic states of the system.

In this thesis, we present data to show that the measurement protocol using a single few-electron quantum dot introduced by Hartman et al. to measure the entropy of a single spin $\frac{1}{2}$ can be extended to measure the entropy of an additional capacitively coupled quantum system. We provide evidence that, when occupation of a single few-electron quantum dot affects the degeneracy of a larger thermodynamic system, the change in entropy of the entire system can be measured while only measuring the occupation of the single quantum dot.

Chapter 2

Entropy in mesoscopic systems

In this chapter, we review the theoretical underpinnings for the measurements that were completed. First, we discuss some of the theory behind single and double quantum dots and the relevant energy scales for these systems. We then proceed to a review of entropy in quantum systems, finally discussing the Maxwell relation used to make the measurements of entropy presented in this thesis and those presented by Hartman et al.

2.1 Entropy of quantum systems

The classical description of entropy comes in the form of the Boltzmann entropy

$$S = k_b \ln W. \quad (2.1)$$

Here, W is defined by the number of available microstates of the system [20]. In the context of simple quantum systems at T close to zero (such that excited states are unattainable), it is useful to consider this quantity, W , as the degeneracy, d , of the ground state of the system [10].

As a simple example, and closely related to the results from this thesis, consider a single potential well that may be occupied by some small number of electrons as illustrated in Fig 2.1(a). In the example outlined Fig 2.1(a), the possible occupations, n , of the well are shown. This system can also be thought of, very approximately, as a model for a single atom with excited states unreachable at low

enough T ¹. In the $n = 0$ state the system has no degeneracy since there is only one state at ground state energy – no electrons anywhere. However, in the $n = 1$ state, the system develops a ground state degeneracy of $d = 2$ since the single electron will be in either a spin up or spin down state, both of which will be of the same energy. Finally, if a second electron is added to the system, the spin degeneracy of the system will break as the lowest energy state of the pair of electrons will be a spin singlet state disallowing net spin freedom of the system.

One can consider the change in entropy, ΔS , of a given transition in the occupation of the potential well² like the transition from $n = 0 \rightarrow n = 1$ as shown in Fig 2.1(b). For this transition, $\Delta S = k_B \ln d_f - k_B \ln d_i = k_B \ln 2$ by Eqn. 2.1

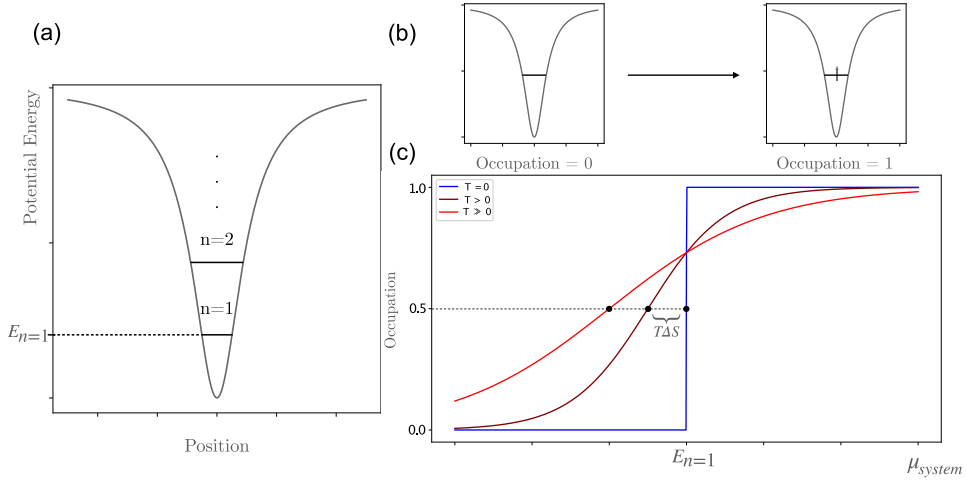


Figure 2.1: In (a) a simple potential well is shown, with the energy levels of various occupations plotted on top of the potential diagram. In (b) and (c) a transition from $0 \rightarrow 1$ electrons in the potential well is illustrated. In (c) finite temperature broadening of this transition, as well as a shift in μ_{system} , due to the change in entropy of the transition, is shown as temperature increases (still much too small to allow for excited states).

Next, we consider the energy at which such a transition would occur, labelled as $E_{n=1}$ for $T = 0$. As temperature is increased, the chemical potential of the system,

¹In practice, potential wells like this can be fabricated on a mesoscopic scale – much larger than any atom – to study the behavior of electrons in “artificial” atoms cf. Ch. 3. These structures are called quantum dots.

²For now, where this electron came from will be neglected.

μ_{system} , at the “half-occupancy” point of such a transition will be affected by the ΔS of the system due to the effect that entropy has on the Helmholtz free energy, F , of a given configuration.

$$F = E - T\Delta S \rightarrow \mu_{\text{sys,transition}} = E_{n=1} - T\Delta S \quad (2.2)$$

Graphically, this effect is shown in Fig 2.1(c), where in addition to an effective broadening of the transition from finite T , the “half-occupancy” point of the transition from $0 \rightarrow 1$ electrons shifts in μ_{system} . It is this affect which we have used in measurements in this thesis to quantify changes in entropy.

2.2 From a Maxwell relation to entropy

The shift in the transition based on a change in entropy as summarized above can be quantified by the following Maxwell relation.

$$\left(\frac{\partial \mu}{\partial T}\right)_{p,N} = -\left(\frac{\partial S}{\partial N}\right)_{p,T} \quad (2.3)$$

Qualitatively, this relation tells us that the change in entropy over the course of a transition in N (e.g. from some N to $N + 1$ particles in a given system) can be expressed in terms of the shift of that transition (in chemical potential) as a function of temperature. As with all the Maxwell relations, there is an additional constant-variable requirement – pressure, p , cannot vary – which will be discussed further in Ch. 3. To further illustrate this qualitative explanation, consider an integral form of the above relation.

$$\Delta S = - \int_{\mu_1}^{\mu_2} \frac{dN(\mu)}{dT} d\mu \quad (2.4)$$

In other words, by measuring the occupation of a system as a function of the chemical potential, $N(\mu)$, and varying temperature, T , one can derive the change in entropy, ΔS over that change in occupation.

In Fig. 2.1, the change in entropy was related to a shift in the mid point of the occupation (of the system) as a function of chemical potential or $N(\mu)$ curve. This shift can also be thought of in terms of the change it would induce in Eqn. 2.4.

If one considers the approximate dN/dT by looking at the difference between a ‘warmer’ and ‘colder’ curve in the figure, it can be noted that, if there is no shift in the center, $\frac{dN}{dT}(\mu)$ will be exactly antisymmetric and therefore integrate to 0. Whereas, in the case that is illustrated, this approximate $\frac{dN}{dT}(\mu)$ is not exactly antisymmetric and will integrate to a finite value.

2.3 Approximate form for a quantum dot coupled to a thermally broadened lead

$$N(\mu, \Theta) = \dots \quad (2.5)$$

$$d \quad (2.6)$$

Chapter 3

Capacitively coupled double quantum dot

This chapter begins with a discussion of quantum dots in GaAs/AlGaAs as well as discussing some of the relevant energy scales when creating double quantum dot systems. Next, the device used for measurements in this thesis is discussed, and the general measurement protocol is outlined. Finally, results are presented.

3.1 The device and measurement protocol

In Ch. 2, the ΔS of transition in a potential well from $0 \rightarrow 1$ electrons was discussed and it was noted that potential wells like the one described could be built in practice by creating something called a quantum dot. Quantum dots can be built from a wide variety of materials [3], and offer a mesoscopic scale realization of something like an “artificial” atom. For measurements in this thesis, tunable quantum dots are fabricated in a 2 dimensional electron gas (2DEG) which forms in an AlGaAs/GaAs substrate. In Fig 3.1 a schematic shows a cross section through such a substrate. When the substrate is cooled to low enough temperature, the bandgap in GaAs and AlGaAs prevents conduction, however, at the interface of the two materials, a sheet of conduction electrons forms which is confined to only two dimension. By adding top gates, as illustrated in Fig 3.1 and applying static voltages to these top gates, this sheet of electrons can be further confined to form many structures including

quantum dots, quantum wires, and quantum point contacts [9].

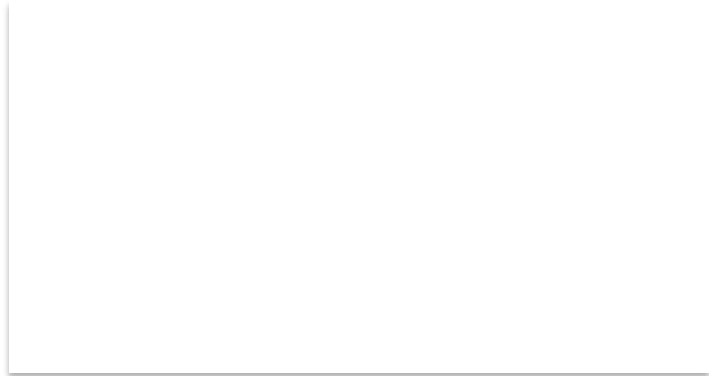


Figure 3.1: A cross sectional view of the AlGaAs/GaAs substrate used in measurements for this thesis. A stack of GaAs and AlGaAs forms a 2DEG at their interface. Ohmic contact is made to the 2DEG by a thermal annealing process with Ni/Au/Ge further discussed in C.2. Gold (Au) top gates are defined on the surface of the substrate which allow for local control of the density of the 2DEG.

To study the entropy of a capacitively coupled system, we have fabricated a double quantum dot system in an AlGaAs/GaAs substrate hosting such a 2DEG. In Fig. 3.1, a top-down image of this device is shown. Two quantum dots are defined, labelled main and impurity dot.

In practice, to measure the entropy of this system using the integral from Eqn. 2.3 we have a few requirements. First, we assumed constant pressure in the Maxwell relation. In the context of a 2DEG with which our measurements are conducted, the dominating pressure at temperatures below the Fermi temperature, $T_F \approx 100\text{K}$ is the degeneracy pressure [2], an incompressibility emerging from the Pauli exclusion principle disallowing fermions from occupying the same quantum state. In addition, by keeping energy fluctuations due to thermal energy, $k_b T$, much smaller than the spacing between energy levels in the dot, we ensure that random temperature fluctuations do not produce unpredictable energy level occupation.

In addition, the primary requirement for using Eqn. 2.4 is the ability to measure occupation of the system as a function of chemical potential while varying temperature. In this device, the occupation of the main dot is the only measured



Figure 3.2: A top-down SEM image of the device measured in this experiment. Lighter gold regions are the gold gates, while darker regions are the GaAs substrate. A single quantum dot (right hand side) is probed by the leftmost dot whose occupation is measured using I_{sense} . In this device, temperature oscillations occur across electrons in a reservoir connected to the probe dot heated via a small thermocurrent through an adjacent quantum point contact. V_{ACC} is used to control the chemical potential, μ , in the probe dot. In the right dot, similar gate structures, labelled V_{IP} allow for the system to be tuned to be tuned degenerate with the probe dot. The X indicates ohmic contact to the 2DEG. The light red section indicates the thermal reservoir of the system. Greyed out gates were not used in this experiment.

quantity¹. We measure N of the main quantum dot by measuring the current I_{sense} through a charge sensing quantum point contact (QPC) seen in Fig. 3.2. Because of the proximity of this QPC, referred to as the charge sensor, to the main dot very small electrostatic changes in the main dot affect the conduction across the charge

¹See Sec. A.3

sensor [5]. As such, a larger I_{sense} indicates fewer electrons in the main dot, while a smaller I_{sense} indicates more electrons in the main dot. In effect, this means that I_{sense} can be used to directly measure the occupancy of the dot as a function of various other quantities like chemical potential, μ , or temperature, T . We use V_{ACC} shown in Fig. 3.2 to locally control the chemical potential of the dot. Varying the electrostatic potential applied to this gate V_{ACC} - and by extension the chemical potential in the dot - is our primary technique to control the occupancy of the dot. Based on this protocol, we can decompose Eqn. 2.4 into the following quantities which can be determined experimentally.

$$\Delta S = - \int_{\mu_1}^{\mu_2} \frac{dN}{dI_{sense}} \frac{dI_{sense}}{dT} d\mu \quad (3.1)$$

This integral tells us that we can measure the change in entropy between two chemical potentials in the dot by measuring two quantities: dN/dI_{sense} , and dI_{sense}/dT as a function of chemical potential. The first quantity, dN/dI_{sense} is just a scaling factor that can be independently experimentally determined and does not depend on μ . In fact, dN/dI_{sense} simply represents the current amplitude of a transition from $N \rightarrow N + 1$ electrons in the dot. The final quantity dI_{sense}/dT does depend on μ and so must be measured as μ is changed. Intuitively, dI_{sense}/dT is a measure of the difference between the occupancy of the dot at higher T and lower T times a scaling factor δT representing the change in temperature.² This difference between hot and cold curves is illustrated by the shading on the plots in Fig. 3.3.

In previous work in the group, Hartman et al. [7] used a very similar process except harnessing Eqn. 2.6 which allows for dI_{sense}/dT to be fit directly so long as the lineshape of the transition is dominated by thermal broadening in the Fermi distribution of the reservoir. Continued work has focussed on extending the single dot findings to less ideal regimes using Eqn 3.1 [4]. However, the remainder of the results and discussion will focus on measurements of entropy in a double quantum dot system.

²See Sec. A.5 for a more in depth consideration of δT in gate voltage.

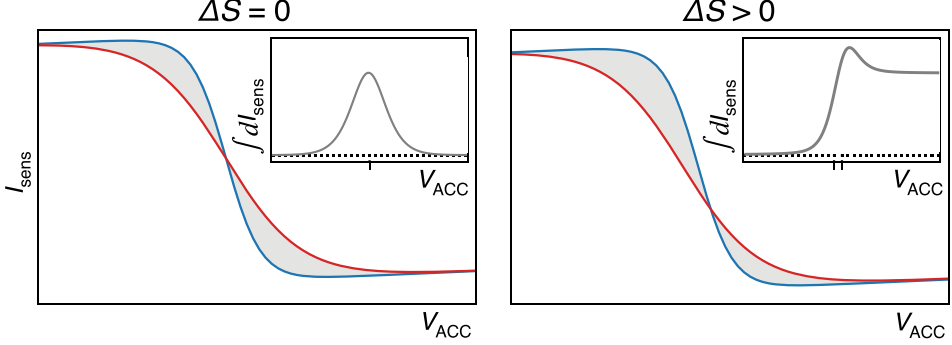


Figure 3.3: In (a) and (b) we show two examples of the measurement protocol where the occupancy of the probe dot is measured using I_{sens} . In each case, the occupancy is swept from $N - 1$ to N electrons both at a higher temperature (red) and a lower temperature (blue), however in (a) this change in N does not correspond to an entropy change in the system whereas in (b) we see a positive change in entropy of the system due to this change in occupancy. The inlaid plots show the cumulative integral of dI_{sens} – or the difference between hot and cold I_{sens} curves. The entropy change of the system is measured by the value of this integral after the completion of this transition. Figure adapted from [7].

3.2 Entropy of a double quantum dot system

In Fig. 3.2, a second quantum dot, labelled impurity dot is shown to the right of the main dot. The occupation of this impurity dot can be tuned by changing the potential on V_{IP} , effectively changing the chemical potential of the dot. Although the charge sensing QPC is farther from this second impurity quantum dot, small changes in I_{sens} can still be detected when the occupation of the impurity dot changes. In Fig. 3.4 the states of the combined system are mapped out by plotting dI_{sens}/dV_{IP} which changes abruptly when occupation shifts occur in either of the dots. The states are labelled by [occupation of main dot, occupation of impurity dot]. Using these transitions, the states of both dots are mapped out over a wide range of gate voltages in Fig. 3.4(a), then zoomed in on the 10, 01 crossing in (b).

In Fig. 3.4 (b), the vertical line jagged indicates a transition in the main dot. Along this transition (as V_{IP} changes) one can consider the change in entropy of the

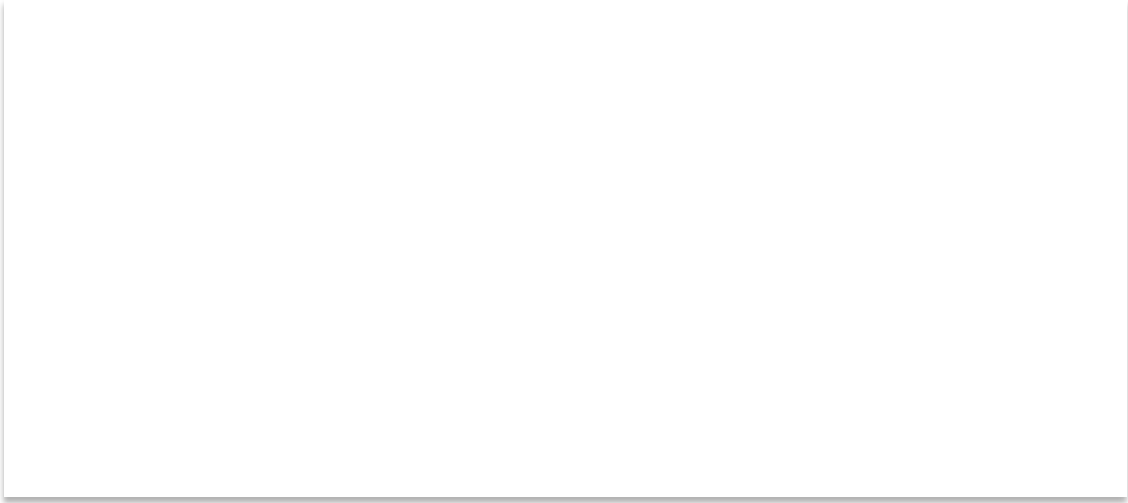


Figure 3.4: In (a) the states of the double quantum dot system are mapped out by charge sensing the occupation of both dots. The color indicates the derivative of the current through the charge sensor. Sudden changes in this current indicate state changes in the two dots, with larger changes (seen as darker on this plot) indicating changes in the main dot, and smaller changes (slightly lighter on this plot) indicating changes in states in the impurity dot. The large squares indicate regions of constant state in the two dots and are labelled by [occupation main dot, occupation impurity dot]. In (b), a zoomed in view on the crossing (white circle in plot (a)) of the $0 \rightarrow 1$ transitions in the two dots is shown.

entire system as the main dot transitions from $0 \rightarrow 1$ electrons shown in Table 3.1 (neglecting charge degeneracy).

Transition	$\Delta S_{sys} [k_B]$	$\Delta S_{main} [k_B]$
$00 \rightarrow 10$	$\ln 2$	$\ln 2$
$01 \rightarrow 10$	0	$\ln 2$
$01 \rightarrow 11$	$\ln 2$	$\ln 2$

Table 3.1: Entropy along 01, 10 transition

Notably, anywhere along this transition, the change in entropy if one considers the main dot only will be $\Delta S = k_B \ln 2$ since it is always transitioning from a no-

occupancy state with no spin degeneracy to a single electron state with a spin degeneracy of two. However, in the case of the $01 \rightarrow 10$ transition, the finite capacitive coupling between the dots causes the impurity dot to be pushed from occupied to unoccupied as the main dot goes from unoccupied to occupied. This implies a clear discrepancy between ΔS_{sys} and ΔS_{main} which will clearly indicate if this protocol continues to work, experimentally, for capacitively coupled systems.

In the case where the impurity dot is tuned to a sufficiently strong tunnel coupling to the reservoir, Γ_{imp} , that the charge degeneracy during the transition is suppressed, the ΔS matches the predicted values for ΔS_{sys} in Table 3.1. This is shown in Fig. 3.5 where over the course of the transition, ΔS goes from $k_B \ln 2$ to 0 then back to $k_B \ln 2$.

In effect, this shows exactly what is expected since thermodynamically, it should not matter what component of the system is being measured if the entire system is undergoing a transition. Another way to understand this is by Fig. 3.5 (c) which shows the transition in occupation of the main dot at various points in the double dot state diagram (a). Each is plotted with both a warm transition and a cold transition. Qualitatively, it is easy to see the relative shift between 50 and 70 mK data like in Fig. 2.1 in the top (purple) transition, however in the center (green) transition, this shift is absent. Although all three transitions are only measurements on the main dot and so are nearly identical regardless of the occupation or change in occupation of the impurity dot, they represent very different state transitions in the system. In the top plot, *only* the main quantum dot is undergoing a transition, whereas in the center plot the larger system is undergoing a transition $01 \rightarrow 10$. Although this larger state transition is not detectable in the $N(\mu)$ curve or as it is collected experimentally, the $I_{sense}(V_{ACC})$ signal, it is clear in the dN/dT signal.

Data was also collected in the case that the impurity dot is less strong coupled to the reservoir, or $\Gamma_{imp}/T < 1$, shown in Fig. 3.6. In this case, charge degeneracy in the impurity dot becomes accessible allowing for states with degeneracy of 3 when the impurity dot is between occupied and unoccupied, and also spin degenerate. In this case, one should theoretically expect to see a $\Delta S_{sys} = \ln 2 - \ln 3 \approx -0.4$ and a $\Delta S_{sys} = \ln 3 \approx 1.1$. In Fig. 3.6(b), theoretical predictions are plotted on top of the experimental data, showing approximate agreement. It is believed the disagreement originates from back action noise affects, which are further summarized

in Sec. A.4

3.3 Conclusion

Not yet sure what the focus of this section will be, still thinking about it.

Figure 3.5: Entropy along the $0,1 \rightarrow 1,0$ transition in the pair of dots with $\Gamma_{main}/T < 1 < \Gamma_{imp}/T$. In (a) the dark region indicates the transition in the main quantum dot. Double dot states are labelled as [Occupation main dot, occupation impurity dot]. The ΔS of the transition in the main dot is plotted for the double dot transition crossing. In the $0,0 \rightarrow 1,0$ regime, the ΔS is found to be roughly $\ln 2 \approx 0.69$ as expected from the spin degeneracy in the probe dot. In the central regime, where there is a full $0,1 \rightarrow 1,0$ transition, entropy is found to be around $\ln 2 - \ln 2 = 0$ since the spin degeneracy of the impurity dot is simply replaced by the spin degeneracy in the probe dot. In (b) the ΔI between the cold and hot curves plotted in (c) are shown. In (c) the shift in V_{mid} between 70 mK and 50 mK traces can clearly be seen to vary depending on ΔS .

Figure 3.6: Entropy along the $0,1 \rightarrow 1,0$ transition in the pair of dots with $\Gamma_{main}/T \approx \Gamma_{imp}/T < 1$. In (a), dI_{sense}/dV_{ACC} indicates the state of both dots as a function of V_{IP} . In (b), theoretical calculations of ΔS are plotted along with the experimental values, error bars showing 95% confidence interval. In (c) dN/dT in units of dI_{sense}/dT is plotted.

Appendix A

Measurement technique

A.1 Heating

The measurement protocol as laid out in Ch. 3 requires the ability to vary the temperature of the system. It was mentioned that this is completed by directly (Joule) heating the electrons in a reservoir coupled to the quantum dot, however the mechanism of this heating was not discussed in depth. In practice, there are a number of limitations that must be considered when constructing a strategy to induce the δT oscillations necessary for entropic measurements as they were completed in this thesis.

The first, and most important, of these limitations is that frequency of the heating, f_{heat} , must be sufficiently large that charge noise in the quantum dot and charge sensor do not affect our determination of dN/dT . Our measurements utilize a continuous measurement of dN/dT as function of chemical potential (see Sec. A.2) however the detrimental affects of a too small f_{heat} can also be understood in the context of repeated measurements of the transition at varying temperatures. If f_{heat} is small, then the ‘period’ of these measurements – time between successive measurements of the transition at different temperatures – will be large. Charge noise in the quantum dot can be thought of as a poisson process and therefore goes as $1/f$ [6]. This means that the larger the time between successive measurements, the more likely a charge jump will occur. Because the protocol relies on the small relative shift between occupation curves at different temperatures, it is exceedingly

sensitive to disturbances in the occupation of the quantum dot between measurements. Effectively, this precludes any heating not localized on the device as it will take too long to equilibrate through the entirety of whatever larger system is being heated.

One way to accomplish localized heating is by directly heating the electrons in the 2DEG using Joule (resistive) heating. It has been shown that, at sufficiently low temperatures, resistive heating can be used to locally raise the temperature of an electron reservoir [11]. Furthermore, in Hartman et al.'s previous work in the group, it was showed that a version of Joule heating worked to effectively heat an electron reservoir and measure entropy. Electrons are heated through a QPC into a narrow channel from a distance of about $5 \mu\text{m}$ from the quantum dot. This heat can quickly thermalize with cold ground ohmic contacts to the channel at either end, but while a current is applied, the temperature of the reservoir can be locally controlled. However, this technique leads to the second difficulty which is that the heating of the reservoir (tunnel) coupled to the quantum dot must *only* change its temperature, and not also change its chemical potential. If the chemical potential of the reservoir is also increased/decreased while heating, it will appear like a relative shift in the center of the transition in the quantum dot. For sufficiently small current biases across this QPC, very little potential builds, and so the 'pure' thermal broadening approximation is valid. However, in the limit of larger current bias, or small dN/dT signal (with respect to this small shift from a change in chemical potential), this technique breaks down. The final complication is that not only can potential in the reservoir coupled to the dot affect the center of transition, but a sufficiently large potential in a nearby reservoir can also induce shifts to the center of the transition. This can most easily be understood as an effective electrostatic gating.

In Fig. A.1 the full schematic for the device used in this thesis is presented. At its most simple level, this represents a two-stage variation of the version outlined in the previous paragraph. In the first stage, electrons are heated by opposing currents through the pair of heating QPCs. By applying an exactly antisymmetric square wave current signal, the affect on the quantum dot of potential in these reservoirs is kept to a dipole moment. Because small potentials will still develop in this first stage, a constriction in the form of another QPC, the 'source', is defined between this first stage at T_{hot} and the next stage, at T_{mid} . It is tuned to about $12 \text{ k}\Omega$, or in

the language of the QPCs, the first plateau¹. Small thermocurrents through this con-

Figure A.1: In (a) the double dot system from measurements in this thesis is shown on a top-down false-color SEM image. In (b) the relation of this device to the other components of the heating apparatus are shown on another top-down SEM image. The two stage heating is labelled by T_{hot} : stage 1, then T_{mid} : stage 2. A number of QPCs control the connection between these stages including the HQPCs which are used for heating, the SQPC which is the source of heat for the second stage, and the DQPC which is the drain for the second stage.

striction allow the second reservoir to heat up in response to changes in temperature in the first without inducing non-negligible potentials in the reservoir coupled to the quantum dot. Finally, a ‘drain’ QPC is used to allow the electrons in the second reservoir to thermalize with a large cold bath of electrons labelled T_{cold} when the heater bias is turned off and the ‘source’ stops supplying heated electrons. In practice, this scheme allows for measurements of entropy in our system while heating with a δT up to a few 100 mK from our base temperature which is usually ≤ 100 mK. Limitations in heating further come from the electron-phonon dissipation of

¹This is a plateau at conductance equal to $2e^2/h$. Conductance is quantized in the ballistic regime through a narrow constriction. The thermal conductivity through QPCs is well studied, a nice summary of the subject can be found here [23].

the heating power which strengthens as T is increased.

A.2 Extraction of dN/dT signal

This section will be devoted to the following topics:

1. The techniques used to allow for repeated measurements and used to fit and extract entropy signals.

A.3 Artifacts from cross couplings

Figure A.2

A.4 Back action noise

A.5 Determination of electron temperature

In the past few sections and in Ch. 3, a great deal of attention was brought to temperature of the system and to oscillations, δT , to the temperature which allow for measurements of dN/dT and subsequently, ΔS . It was stated that the temperatures

can be exactly determined by thermal broadening of the Fermi distribution in the reservoir, and in particular Eqn. 2.5 was referenced as a means of calculating the exact broadening of the Fermi distribution by the broadening of the lineshape of the occupation ($N(\mu)$) curve. In this section, this assumption is experimentally justified and an approximate base electron temperature is established.

To start, consider an experimental form of Eqn. 2.5 to allow for direct fitting to data as it is collected – I_{sense} as a function of V_{ACC} [7].

$$I_{sense}(\Theta, V_{ACC}) = I_0 \tanh\left(\frac{V_{ACC} - V_{mid}(\Theta)}{2\Theta}\right) + \gamma V_{ACC} + I_1 \quad (\text{A.1})$$

Where I_0 represents the amplitude of the transition in terms of current, V_{mid} the center of the transition in terms of gate voltage, and I_1 , the current at the center point of the transition. The (constant) γ term allows for an effective linear cross capacitance between V_{ACC} and the current through the charge sensor. In this context, Θ gives the thermal broadening of the transition in gate voltage. Importantly, $\Theta \propto k_B T$.

In Fig. A.3, the temperature of the mixing chamber (MC) plate on which the sample is mounted is varied, and repeated measurements of the transition (two examples shown in (b)) are acquired. Each is fit to Eqn. A.1 yielding a value Θ in mV which is plot in Fig. A.3(a). For the majority of the plot, as expected, the thermal broadening of the transition, represented by Θ , goes like T . Therefore, in the linear regime, it is quite clear that any temperature oscillation δT will be proportional to a $\delta\Theta$.

It is useful to also consider the deviation in Θ away from this linear fit at very low T . This is a byproduct of a combination of radiation increasing the temperature of the electrons and weak electron-phonon coupling. It is a well known effect [24], and thus the most experimentally important metric about any given cryogenic system operating at mK temperatures is the effective base electron temperature, and not the the base lattice temperature. The non-linearity in the Θ vs T curve, then, is a result of this deviation between electron and lattice temperature, since $\Theta \propto k_B T_e$. By extrapolating the linear $\Theta(T)$ curve to smaller Θ , we can conclude that the effective base T_e is about 35mK at our base fridge temperature.

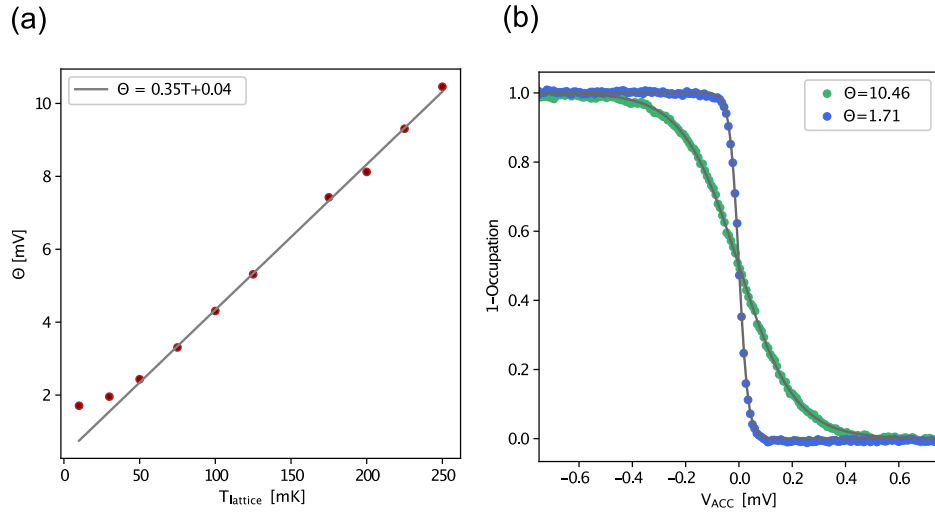


Figure A.3: By fitting the transition line shapes of the $0 \rightarrow 1$ electron transition in the quantum dot, one can extract the broadening of the fermi energy in the reservoir. By varying the lattice temperature of the substrate and plotting the effective broadening of the fermi sea (Θ) at each lattice temperature, we can extract the effective electron temperature, T_e . Here $T_{e,\text{base}} \approx 35$ mK.

Appendix B

Measurement setup

To make the measurements in this thesis, a great deal of work was put into developing a low noise wiring solution for the low frequency DC measurements necessary for measuring entropy in our devices. Because of the work of many previous students, nearly all of the instrumentation used as well as power supplies for these instruments have already been heavily optimized.

Specifically the instrumentation used was, for DC data acquisition as well gathering the device, a modified openDACs DAC-ADC in conjunction with a Basel Precision Instruments current pre-amplifier.¹ Both instruments are powered by a low noise isolation transformer paired with inverters.

Measurements were completed in a dry dilution refrigerator – Bluefors XLD Dilution Refrigerator. A well known problem with dry systems is that their use of a pulse tube cryocooler induces a large amount of vibrational noise. It is thought that these vibrations can induce electrical noise in the measurement lines due to a triboelectric mechanism [8, 13, 15]. Effectively, this is the same mechanism that induces static charge when two surfaces are rubbed together. A possible explanation of the effect is that insulators around the actual measurement lines rub against either the conductors themselves, inducing a charge and thus, a small current, or rub against other surfaces inducing an image charge in the conductor. Regardless of

¹ Available at <http://opendacs.com> and <https://www.baspi.ch> respectively. Modified openDACs source code was developed by members of the lab, Tim Child and Christian Olsen, in conjunction with Mark Carlsen. Available at <https://github.com/folk-lab/FastDAC>

the explanation, the experimental reality is that in dry dilution systems, one must be very careful to limit the effects of triboelectric noise. In particular, in worse configurations of the wiring and the same instrumental configuration we have seen up to 100x (over a 1kHz bandwidth) the base noise level reported in Fig. B.1 dominated by broad spectrum vibrational resonances and not 60 Hz plus multiples.

Figure B.1: In (a) a current PSD and its integral for an open line are plotted indicating an open line noise of about $200 \text{ fA}/\sqrt{\text{Hz}}$ in the $0 \rightarrow 1 \text{ kHz}$ bandwidth. Notably, the majority of the remaining noise can be attributed to a contribution at 400 Hz which we attribute to a vibrational resonance in our wiring. In (b), the coldfinger design utilized for this low noise setup is imaged. Flat flexible cables are used to connect the wiring to a set of RC filters on the face of the MC plate (top of picture). These cables are spray-coated in a thin layer of graphite which limits vibrations from inducing triboelectric noise in the cables.

As a consequence of the difficulty of limiting triboelectric noise, a number of iterations of wiring were developed with the current iteration shown in Fig. B.1 (b). Twisted pair Ph-Br unshielded wiring was used from the top of the fridge to the MC plate (shown in the top of Fig. B.1(b)). This wiring was hand-soldered to a 3-pole RC filter with $f_{char} \approx 60 \text{ kHz}$. The stages in the filter are 500 Ohm, 2×47

pF, 500 Ohm, 2 x 220 pF, and 500 Ohm, 2 x 820 pF. Grounding for this RC filter is defined at the top of the fridge through a separate line. From this filter to the base of the coldfinger a narrow flat flexible kapton + BeCu conductor cable is utilized. This flat flexible cable is coated in a thin layer of graphite to conduct any charge developing from triboelectric effects away. It is then clamped to the coldfinger to limit vibrational noise.

Appendix C

Device Fabrication

To fabricate the devices referred to in this thesis and previous iterations of similar devices, a number of nano-fabrication recipes were developed and iterated upon. In this section, these processes are described and recipes used are laid out.

C.1 Summary

There are two key features to devices built on GaAs/AlGaAs 2DEGs – ohmic contact to the 2DEG and gating structures. In overview, devices used for this project use a thin film of Al_2O_3 to electrically isolate top-gates fabricated from Au/Pd. Ohmic contacts are made using annealed Ni/Au/Ge. In Fig. C.1 a number of the key steps in these processes are illustrated.

The general process of preparation of a sample goes as follows:

1. Gallium removal from back of wafers.
2. Ohmic contact: lithography, evaporation, annealing.
3. Mesa etching: lithography, $\text{H}_2\text{S}\text{O}_4$ etching.
4. Atomic layer deposition: Al_2O_3 .
5. Gating (2 steps): lithography, evaporation.

C.2 Recipes

C.2.1 Gallium removal

This process is described for completeness, however this recipe was not developed, or iterated on, with my help. This is a recipe developed by Dr. Silvia Luescher Folk.

1. Cleave a full wafer into a quarter or half wafer. Blow off any dust bunnies from the surface before starting.
2. Spin a layer of AZ1518 resists at 4000 RPM for 40s.
3. Bake the resist for 2min at 100C.
4. Put a clean wipe on a hotplate and set to 50C. Put wafer face down (gallium side up) onto the clean wipe.
5. Wipe off gallium with q-tips. Keep wiping until it is all gone.
6. Spin and bake another layer of AZ1518 (4000 RPM 40s and bake 100C 2min).
7. Etch 2 min in full strength HCl. Quench etch by transferring to DI water.
8. Rinse well in DI water. Blow-dry.
9. Squirt down with Acetone to strip resist from the surface and immediately rinse with IPA.
10. Soak 3min each in Toluene, Acetone, and IPA. Rinse with IPA and blow dry between each solvent. Spray down with DI water and blow-dry.

C.2.2 Mesa Etch

1. Solvent clean – Acetone, IPA. Rinse in DI, blow dry with N₂.
2. Prebake chip for 2 min at 180C
3. PMMA A4 950K at 4000 rpm for 40s with a 3 min postbake at 180C.

4. E-beam lithography in Jeol JBX-8100FS
5. Develop in IPA:DI, 7:3 40s at 18C, stop develop in DI
6. O₂ plasma etch in Plasma-etch PE-50, 40s
7. Etch in 30 mL diluted Sulfuric acid (700 Water:3 H₂S0₄) + 3 mL H₂O₂ at 18C for an etch rate of about 5nm/s.
8. Stop etch in DI water. Remaining resist can be removed with Acetone.

C.2.3 Ohmic contact

Lithography and Evaporation: The following steps have been shown to be capable of making usable ohmic contacts of contact resistances of about 1 kΩ, however continued work has been focussed on optimizing the recipe for further use.

1. Solvent clean – Acetone, IPA, Ultrasound. Rinse in DI, blow dry with N₂.
2. Prebake chip for 2 min at 180C
3. Spin MMA/PMMA A4 950K bilayer at 4000 rpm for 40s each with a 3 min postbake at 180C after each layer.
4. E-beam lithography in Jeol JBX-8100FS at a dose of 450 μC/cm².
5. Develop in IPA:DI, 7:3 40s at 18C, stop develop in DI
6. O₂ plasma etch in Plasma-etch PE-50, 15s
7. Evaporate the following:

Metal	Thickness	Rate
Ni	5nm	1.3Å/s
Au	68nm	1.7Å/s
Ge	68nm	1Å/s
Au	68nm	2Å/s
Ni	50nm	1.6Å/s
Au	50nm	2.2Å/s

Table C.1: Evaporation for ohmics

8. Liftoff in Acetone at room temperature.

Annealing: The following process was followed on the rapid thermal annealer made “in-house” for annealing GaAs and other substrates. The basic idea is to use a bulb in a near vacuum (with some amount of forming gas – H₂ + N₂) to heat the sample to a high temperature for a limited amount of time. The metal film melts and sinks into the GaAs substrate to make contact with the 2DEG which is usually 30-200nm below the surface. A sample of a chip before and after annealing can be seen in Fig. [C.1].

1. Pump down should reach lower limit, 0.133 mbar
2. Set regulator to 2.5 psi (forming gas)
3. Open Swagelock valve until pressure reads 10mbars
4. Close speedivalve until pressure reads 200mbar
5. Turn on bulb to roughly 34%, it takes about 5-10 minutes
6. Wait at 350C for 2min
7. Go to 450C as fast as you can, hold it there for 40s
8. Cool below 300C fast by opening the speedivalve on the pump line all the way, and opening the gas flow.
9. Cool to 50C, then vent and let cool to room temp

C.2.4 Gating

Inner gates

1. Solvent clean – Acetone, IPA. Rinse in DI, blow dry with N₂.
2. Prebake chip for 3 min at 180C.
3. PMMA A2 at 4000 rpm for 40s with a 3 min postbake at 180C.

4. E-beam lithography in Jeol JBX-8100FS
5. Develop in IPA:DI, 7:3 40s at 18C, stop by directly drying with N2
6. Evaporate Pd 2nm, 0.8Å/s then Au 12nm, 1Å/s
7. Liftoff in Acetone at room temperature.

Outer gates and bondpads

1. Solvent clean – Acetone, IPA. Rinse in DI, blow dry with N₂.
2. Prebake chip for 3 min at 180C.
3. Spin MMA/PMMA A4 950K bilayer at 4000 rpm for 40s each with a 3 min then 7 min postbake at 180C after each layer.
4. E-beam lithography in Jeol JBX-8100FS
5. Develop in IPA:DI, 7:3 40s at 18C, stop in DI
- 6.
7. O₂ plasma etch in Plasma-etch PE-50, 1 min
8. Evaporate Ti 10nm, 2Å/s then Au 150nm, 4Å/s
9. Liftoff in Acetone at room temperature.

C.2.5 Disclaimer

Although a number of working devices were fabricated according to this process, initial fab on the GaAs/AlGaAs 2DEG used for the final measurements in this thesis was completed before this project began. Christian Olsen's thesis available here:

<https://www.nbi.ku.dk/english/theses/masters-theses/christian-olsen/Olsen.CH.Master.pdf>
describes in detail the exact process used to complete all but the gating of this 2DEG, which was completed following the recipes above.

Figure C.1: In (a), a sample chip is shown (optical image) before (L) and after (R) annealing. Notably, the process of annealing melts the metals that were evaporated onto the surface of the chip, forming an alloy. The change in surface quality of the metal between the two images shows that this process has occurred. In (b) and (c) a sample pair of optical images show a sample with resist having already been written (b) and this same chip post evaporation (c). In (d), a schematic side view of the lithography process is shown. PMMA forms concave side walls preventing the metallic film from making contact with the substrate, except in areas defined by an electron beam. After a state like that shown in (d) is reached, Acetone can be used to “liftoff” the unneeded metallic film by dissolving the PMMA on which the metallic film is resting.

Bibliography

- [1] Fault-tolerant quantum computation by anyons. *Annals of Physics*, 303(1):2 – 30, 2003. ISSN 0003-4916.
[doi:`https://doi.org/10.1016/S0003-4916\(02\)00018-0`](https://doi.org/10.1016/S0003-4916(02)00018-0). → pages [1]
- [2] N. W. Ashcroft and N. D. Mermin. *Solid State Physics*. Holt, Rinehart & Winston, New York ; London, 1976. → pages [8]
- [3] D. Bera, L. Qian, T.-K. Tseng, and P. H. Holloway. Quantum dots and their multimodal applications: a review. *Materials*, 3(4):2260–2345, 2010. → pages [7]
- [4] T. Child, O. Sheekey, N. Hartman, S. Lüscher, J. Folk, S. Fallahi, G. Gardner, and M. Manfra. Entropy measurements in mesoscopic circuits: opportunities and limitations. *Bulletin of the American Physical Society*, 65, 2020. → pages [10]
- [5] J. Elzerman, R. Hanson, L. W. Van Beveren, B. Witkamp, L. Vandersypen, and L. P. Kouwenhoven. Single-shot read-out of an individual electron spin in a quantum dot. *nature*, 430(6998):431–435, 2004. → pages [10]
- [6] T. Fujisawa and Y. Hirayama. Charge noise analysis of an algaas/gaas quantum dot using transmission-type radio-frequency single-electron transistor technique. *Applied Physics Letters*, 77(4):543–545, 2000. → pages [17]
- [7] N. Hartman, C. Olsen, S. Lüscher, M. Samani, S. Fallahi, G. C. Gardner, M. Manfra, and J. Folk. Direct entropy measurement in a mesoscopic quantum system. *Nature Physics*, 14(11):1083–1086, 2018. → pages [vii, 1, 10, 11, 21]
- [8] R. Kalra, A. Laucht, J. P. Dehollain, D. Bar, S. Freer, S. Simmons, J. T. Muhonen, and A. Morello. Vibration-induced electrical noise in a

- cryogen-free dilution refrigerator: Characterization, mitigation, and impact on qubit coherence. *Review of Scientific Instruments*, 87(7):073905, 2016. → pages [23]
- [9] M. J. Manfra. Molecular beam epitaxy of ultra-high-quality algaas/gaas heterostructures: enabling physics in low-dimensional electronic systems. *Annu. Rev. Condens. Matter Phys.*, 5(1):347–373, 2014. → pages [8]
- [10] D. A. McQuarrie. *Statistical Mechanics*. University Science Books, 2000. → pages [3]
- [11] A. Mittal, R. Wheeler, M. Keller, D. Prober, and R. Sacks. Electron-phonon scattering rates in gaas/algaas 2deg samples below 0.5 k. *Surface Science*, 361:537–541, 1996. → pages [18]
- [12] V. Mourik, K. Zuo, S. M. Frolov, S. R. Plissard, E. P. A. M. Bakkers, and L. P. Kouwenhoven. Signatures of majorana fermions in hybrid superconductor-semiconductor nanowire devices. *Science*, 336(6084): 1003–1007, 2012. ISSN 0036-8075. doi:10.1126/science.1222360. → pages [1]
- [13] E. Mykkänen, J. Lehtinen, A. Kemppinen, C. Krause, D. Drung, J. Nissilä, and A. Manninen. Reducing current noise in cryogenic experiments by vacuum-insulated cables. *Review of Scientific Instruments*, 87(10):105111, 2016. → pages [23]
- [14] C. Nayak, S. H. Simon, A. Stern, M. Freedman, and S. Das Sarma. Non-abelian anyons and topological quantum computation. *Rev. Mod. Phys.*, 80:1083–1159, Sep 2008. doi:10.1103/RevModPhys.80.1083. → pages [1]
- [15] M. Pelliccione, A. Sciambi, J. Bartel, A. Keller, and D. Goldhaber-Gordon. Design of a scanning gate microscope for mesoscopic electron systems in a cryogen-free dilution refrigerator. *Review of Scientific Instruments*, 84(3): 033703, 2013. → pages [23]
- [16] I. Pomeranchuk. On the theory of liquid 3he. *Zh. Eksp. Teor. Fiz.*, 20:919, 1950. → pages [2]
- [17] R. M. Potok, I. G. Rau, H. Shtrikman, Y. Oreg, and D. Goldhaber-Gordon. Observation of the two-channel kondo effect. *Nature*, 446(7132):167–171, 2007. doi:10.1038/nature05556. → pages [1]

- [18] A. Rozen, J. M. Park, U. Zondiner, Y. Cao, D. Rodan-Legrain, T. Taniguchi, K. Watanabe, Y. Oreg, A. Stern, E. Berg, P. Jarillo-Herrero, and S. Ilani. Entropic evidence for a pomeranchuk effect in magic-angle graphene. *Nature*, 592(7853):214–219, 2021. doi:10.1038/s41586-021-03319-3 URL <https://doi.org/10.1038/s41586-021-03319-3>. → pages [2]
- [19] Y. Saito, F. Yang, J. Ge, X. Liu, T. Taniguchi, K. Watanabe, J. I. A. Li, E. Berg, and A. F. Young. Isospin pomeranchuk effect in twisted bilayer graphene. *Nature*, 592(7853):220–224, 2021. doi:10.1038/s41586-021-03409-2 URL <https://doi.org/10.1038/s41586-021-03409-2>. → pages [2]
- [20] D. Schroeder. *An Introduction to Thermal Physics*. Addison Welsley Longman, 2000. → pages [3]
- [21] E. Sela, Y. Oreg, S. Plugge, N. Hartman, S. Lüscher, and J. Folk. Detecting the universal fractional entropy of majorana zero modes. *Phys. Rev. Lett.*, 123:147702, Oct 2019. doi:10.1103/PhysRevLett.123.147702 → pages [1]
- [22] Z. Su, A. Zarassi, J.-F. Hsu, P. San-Jose, E. Prada, R. Aguado, E. J. H. Lee, S. Gazibegovic, R. L. M. Op het Veld, D. Car, S. R. Plissard, M. Hocevar, M. Pendharkar, J. S. Lee, J. A. Logan, C. J. Palmstrøm, E. P. A. M. Bakkers, and S. M. Frolov. Mirage andreev spectra generated by mesoscopic leads in nanowire quantum dots. *Phys. Rev. Lett.*, 121:127705, Sep 2018. doi:10.1103/PhysRevLett.121.127705. → pages [1]
- [23] H. Van Houten and C. Beenakker. Quantum point contacts. *arXiv preprint cond-mat/0512609*, 2005. → pages [19]
- [24] F. C. Wellstood, C. Urbina, and J. Clarke. Hot-electron effects in metals. *Phys. Rev. B*, 49:5942–5955, Mar 1994. doi:10.1103/PhysRevB.49.5942 URL <https://link.aps.org/doi/10.1103/PhysRevB.49.5942>. → pages [21]
- [25] R. Willett, J. P. Eisenstein, H. L. Störmer, D. C. Tsui, A. C. Gossard, and J. H. English. Observation of an even-denominator quantum number in the fractional quantum hall effect. *Phys. Rev. Lett.*, 59:1776–1779, Oct 1987. doi:10.1103/PhysRevLett.59.1776. → pages [1]